Pressure-constrained deformation and superior strength: Compressed graphite versus diamond

Wei Zhou,[1,2] Hong Sun,[1,2,*] Yi Zhang,[2] and Changfeng Chen[2,†]

[1]*Department of Physics and Astronomy and Key Laboratory of Artificial Structures and Quantum Control (Ministry of Education), Shanghai Jiao Tong University, Shanghai 200240, China*

[2]*Department of Physics and High Pressure Science and Engineering Center, University of Nevada, Las Vegas, Nevada 89154, USA*

(Received 10 September 2012; revised manuscript received 14 November 2012; published 30 September 2013)

We show by first-principles calculations that high-pressure confinement suppresses the usual ambient or low-pressure deformation modes for compressed graphite toward low-density phases under large shear deformation and promotes alternative structural evolution to high-density phases that possess enhanced shear strength surpassing that of diamond. This finding explains the puzzling experimental observation of compressed graphite cracking diamond anvil [W. L. Mao *et al*., Science **302**, 425 (2003)] and suggests different principles for determining material strength at high pressure. It also underscores the need to go beyond empirical hardness formulas that are unable to account for changes in pressure-constrained structural evolution and their influence on strength.

DOI: 10.1103/PhysRevB.88.104111 PACS number(s): 61.50.Ks, 61.66.Bi, 62.20.−x, 81.40.Jj

Shear deformation in a crystal is a key mechanism for incipient plasticity and structural instability. Studies of structural deformation under shear strains have played an essential role in understanding phase transformation, dislocation generation, and material strength.[1–9] Here we examine shear deformation modes of a distinct type of carbon allotropes synthesized under cold compression.[10–12] A pressure-induced structural transformation turns soft graphite into a superhard compressed phase that can crack the diamond anvil cell (DAC).[12] This has stimulated great interest in identifying the structure of compressed graphite and the mechanism underlying its superior strength exceeding that of diamond. Extensive recent studies have identified a variety of possible compressed graphite phases[13–24] that can be classified into structures with 6, $5+7$, $4+8$ membered ring topologies or their mixtures. Ideal shear strength calculations can predict incipient plasticity in a crystal[9] and determine the lowest shear stress needed to destabilize a perfect crystal, thus setting an upper bound for material strength. This makes ideal shear strength a benchmark quantity in assessing material strength and hardness; it is especially useful in a comparative study of different materials. Recent calculations indicate, however, that compressed graphite phases exhibit strength lower than that of diamond,[25,26] which directly contradicts the experimental observation, leaving the superior strength of compressed graphite unexplained.

In this paper, we explore shear deformation modes and strength of compressed graphite by extending ideal shear strength calculations to include the effect of pressure constraint in DAC, which is the major factor omitted in previous calculations. Here we focus on three representative cases, W-carbon,[15] M-carbon,[13] and Z-carbon,[17,18] which have $5+7$ and $4+8$ membered ring topologies, respectively, and compare them with diamond that has a 6-membered ring topology. We show that high-pressure confinement suppresses structural transformations of these carbon allotropes to low-density phases that exist at ambient or low pressure and promotes alternative transformation pathways to high-density phases with shear strength higher than that of diamond. Similar trends are expected for all proposed compressed graphite carbon allotropes that have $5+7$ and $4+8$ membered ring topologies. This explains the puzzling experimental observation of compressed graphite cracking diamond and reveals fundamental changes in the deformation mechanism during pressure-constrained structural evolution. It also highlights the need to go beyond empirical hardness formulas[27–30] that are unable to accurately describe the strength-pressure relation of compressed graphite.

We used the VASP code,[31] adopting the projector augmented wave (PAW) potentials[32] and local-density approximation (LDA) with the exchange-correlation functional of Ceperley and Alder[33] as parametrized by Perdew and Zunger.[34] We minimized the total energy using a conjugate gradient optimization method[35] and employed a $10\times14\times6$ (and $11\times11\times11$ for diamond) Monkhorst-Pack[36] k-point grid and a 550 eV energy cutoff, achieving an energy convergence on the order of 1 meV per atom and residual forces and stresses less than 0.005 eV/Å and 0.1 GPa, respectively. The ideal shear strength and relaxed loading path were determined using a previously established method[6,7] with modifications to include the pressure effect. The lattice vectors were incrementally deformed in the direction of applied shear strains, say τ_{xz}. At each step, the applied shear strain is fixed to determine the shear stress σ_{xz}, while the other five independent components of the strain tensors and all the atoms inside the unit cell were simultaneously relaxed until (i) the normal components (σ_{xx}, σ_{yy}, σ_{zz}) of the stress tensor all equal the applied pressure, (ii) the two independent shear components (σ_{xy}, σ_{yz}) of the stress tensor are negligibly small (less than 0.1 GPa), and (iii) the force on each atom becomes negligible (less than 0.005 eV/Å). The shape of the (deformed) unit cell, the positions of the atoms and the relation between the shear stress σ_{xz} and shear strain τ_{xz} are determined completely at each step by this pressure-constrained atomic relaxation procedure.

We carried out an extensive investigation of shear deformation and strength of W-carbon, M-carbon. and Z-carbon by performing stress-strain calculations in all inequivalent {001}, {011}, and {111} planes sheared along all the edge and diagonal directions in each plane at selected hydrostatic pressures (totaling 796 full stress-strain calculations). The results are summarized in Fig. 1 and compared to the lowest peak

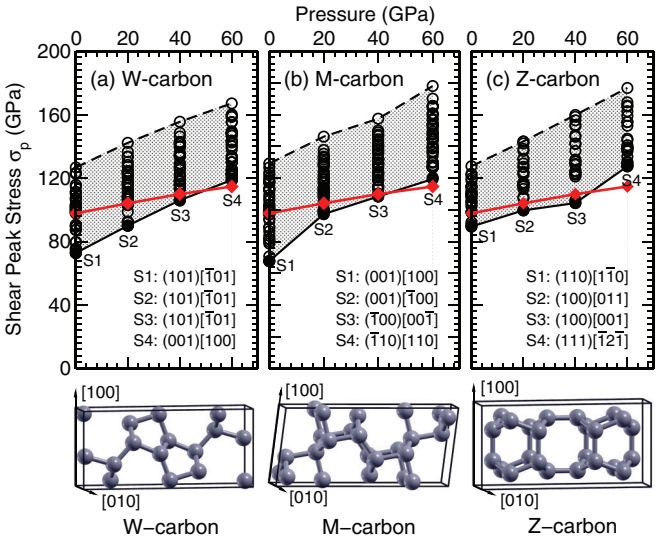

FIG. 1. (Color online) Calculated shear peak stresses (circles) in all inequivalent {001}, {011}, and {111} planes for (a) W-carbon, (b) M-carbon, and (b) Z-carbon under hydrostatic pressure, where $S1, \ldots, S4$ indicate the shear directions with the lowest peak stress at different pressures, compared to the lowest peak stress of diamond (diamond symbols) in its (111)[11$\bar{2}$] shear direction. Structures of W-carbon, M-carbon, and Z-carbon are also shown.

stress of diamond in its (111)[11$\bar{2}$] shear direction. A distinct feature of structural evolution for these carbon allotropes in shear deformations under high-pressure confinement is that, unlike at ambient pressure, deformed structures are less likely to graphitize, leading to alternative transformation pathways toward high-density phases with enhanced shear strengths (see discussions below for more details). As pressure approaches 60 GPa, the lowest shear peak stresses (i.e., the ideal shear strengths) of W-carbon, M-carbon, and Z-carbon all become higher than that of diamond. It is noted that the nominal pressure for the transformation of graphite to the compressed phase is about 17 GPa;[12] it has been shown,[37] however, that pressure distribution inside a DAC is highly inhomogeneous, and at an average pressure of 17 GPa, local stress near the edge of the graphite sample in DAC, where the crack in diamond anvil appears, can exceed 100 GPa, which is well above the threshold pressure (near 60 GPa) suggested by our calculations. These results provide the first quantitative explanation for the experimental observation of graphite cracking diamond anvil.

To understand the shear deformation process, we examine the calculated stress-strain curves and the corresponding changes of the enthalpy and unit cell volume. Here we focus on W-carbon and M-carbon since they are considered the most probable carbon allotropes of compressed graphite.[23,24] We compare the results at relatively low pressure of 20 GPa, where the proposed compressed graphite phases become more stable than graphite,[19,20] and those at 60 GPa, where the strength of compressed graphite exceeds that of diamond. The results of W-carbon are presented in Fig. 2. We track two particular shear deformation modes of interest here, viz., the weakest shear directions of W-carbon at 20 GPa ($S2$: (101)[$\bar{1}$01]) and 60 GPa ($S4$: (001)[100]). Along $S2$ W-carbon has a peak stress of 90.0 GPa at shear strain $\tau = 0.245$, which is below the lowest peak stress (102.3 GPa) of diamond at 20 GPa. At $\tau = 0.27$ ($L1$ point) beyond the peak strain, W-carbon transforms into a low-density structure with an expansion of its unit cell volume, which is a common behavior in strong covalent solids at ambient pressure.[3,4] At high pressure (60 GPa), however, this transformation to the low-density phase is suppressed since the expansion of the volume would increase the enthalpy ($H = E + pV$) of the structure more significantly than at lower pressure. Consequently, an alternative deformation pathway develops along $S2$, leading to a high-density phase (see structure $H1$ in Fig. 2) at a larger strain $\tau = 0.325$ ($H1$ point) with an enhanced peak stress of 122.3 GPa at $\tau = 0.305$, which is higher than the lowest peak stress of diamond (114.7 GPa) at the same pressure (60 GPa).

The difference in deformation modes at low (20 GPa) and high (60 GPa) pressure is also reflected in the calculated enthalpy. In the former case, the drop in energy due to bond breaking is largely compensated by the volume expansion, resulting in only a slight decrease of enthalpy at the $L1$ point, while the nearly constant volume in the latter case leads to a much larger enthalpy decrease upon rebonding at the $H1$ point. A notable development here is that $S2$ actually is no longer the weakest shear direction at 60 GPa. Instead, the easy shear deformation now proceeds along $S4$. A distinct feature of this pathway is that the transformation to a low-density phase, which appears at zero pressure (not shown here), is suppressed at relatively low pressures. This is the case even at 20 GPa where W-carbon shows the first peak stress (91.8 GPa) at $\tau = 0.23$ and then transforms into a high-density phase with a smaller unit cell volume at $\tau = 0.25$ ($L2$ point), which has a (second) peak stress (106.6 GPa at $\tau = 0.62$) that is higher than the lowest peak stress (102.3 GPa) of diamond at the same pressure (20 GPa). At high pressure (60 GPa), it becomes the weakest shear direction of W-carbon. The high-pressure constraint directs W-carbon to transform into a high-density phase at $\tau = 0.275$ ($H3$ point) with slightly decreased volume and a peak stress of 118.8 GPa at $\tau = 0.26$ that is higher than the lowest shear peak stress (114.7 GPa) of diamond at the same pressure. Our calculated results show that such pressure-constrained multistage transformation among high-density phases becomes commonplace for compressed graphite in shear deformation as pressure increases. It is interesting to note, however, that such suppression of transformation to low-density phases by pressure does not happen for diamond. In its weakest direction (111)[11$\bar{2}$], diamond transforms into low-density phases (i.e., graphitizes) under both low (20 GPa, $L'1$ point) and high (60 GPa, $H'1$ point) pressures. This reflects that for diamond the energy reduction due to bond breaking (from sp^3 to sp^2) exceeds the increase in the pV term in enthalpy due to the volume expansion even at 60 GPa. The relatively minor role of volume expansion here is also seen in the considerable enthalpy drop at $L'1$ and $H'1$ points, albeit becoming smaller at higher (60 GPa) pressure as the contribution from the pV term increases.

The results for M-carbon (see Fig. 3) are similar. At low pressure (20 GPa), the weakest shear direction is (001)[$\bar{1}$00], and a transformation into a low-density phase occurs at $\tau = 0.295$ ($L1$ point) with a peak stress of 99.4 GPa, which is lower than that (102.3 GPa) of diamond in its weakest shear

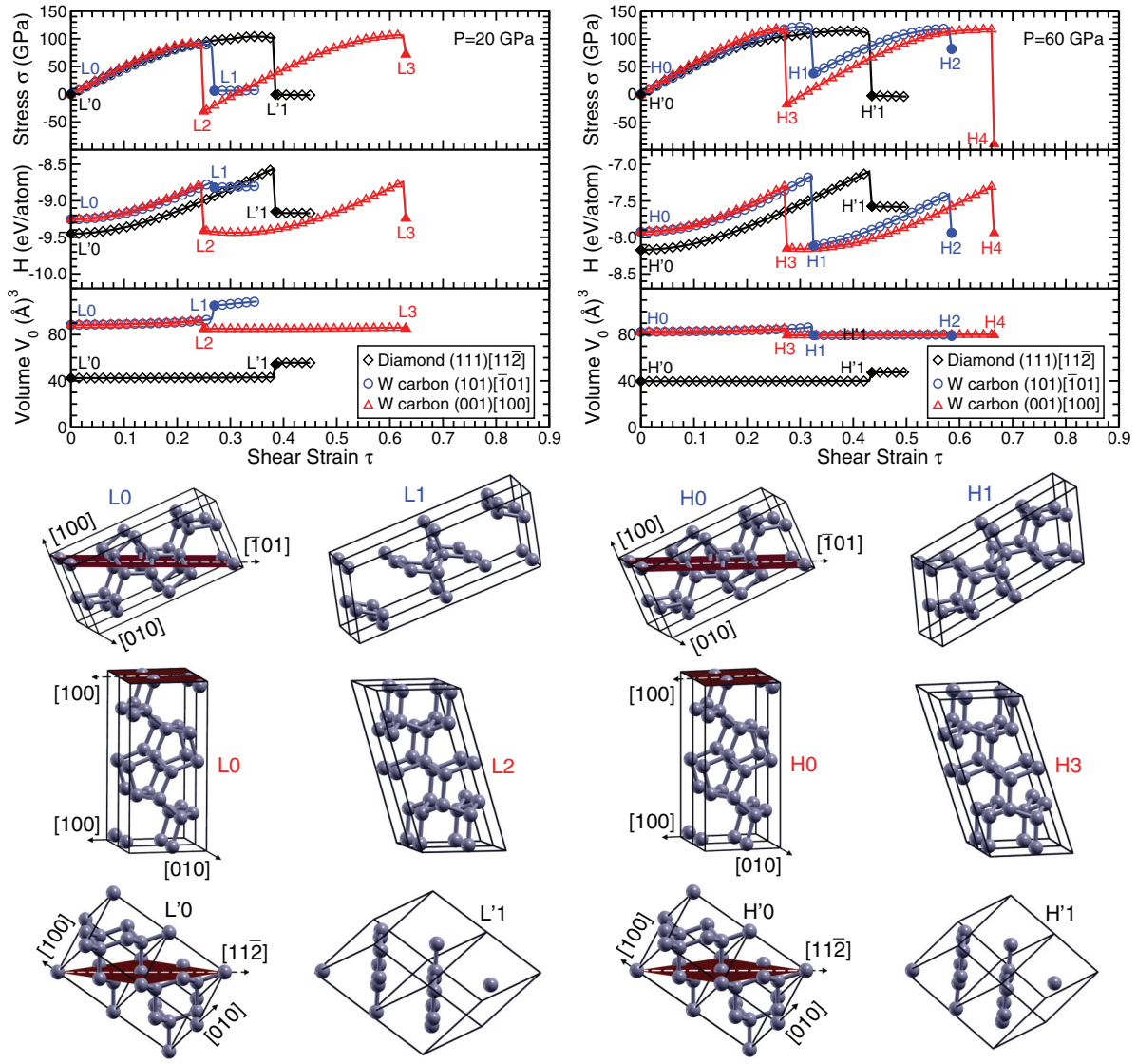

FIG. 2. (Color online) Calculated stress (upper panel), enthalpy (middle panel), and unit cell volume (lower panel) of W-carbon versus strain in the (101)[$\bar{1}$01] and (001)[100] shear directions (shear sliding planes are shaded) at 20 and 60 GPa compared to those of diamond in the (111)[11$\bar{2}$] shear direction. Also given are selected structural snapshots of W-carbon and diamond during shear deformation. The unit cell of W-carbon (diamond) contains 16 (8) carbon atoms.

direction. This transformation to a low-density phase is again suppressed at high pressure (60 GPa), and the transformation along (001)[$\bar{1}$00] redirects M-carbon to a high-density phase at $\tau = 0.32$ ($H1$ point) that has a high peak stress of 134.0 GPa. At high pressure (60 GPa), the weakest shear direction of M-carbon changes to ($\bar{1}$10)[110] that has a peak stress of 120.3 GPa, which is still higher than the lowest shear peak stress (114.7 GPa) of diamond at the same pressure.

Z-carbon exhibits similar results (not shown here) with the same trend showing that high pressure suppresses transformations to low-density phases under shear deformation and promotes high-density phases with increased shear strengths surpassing that of diamond. These compressed graphite phases share a common structural feature, namely their $5+7$ or $4+8$ membered ring structures allow more flexibility for variations in bond length and angle, resulting in weaker C-C bonds (than those in diamond). Such bonds break earlier at low pressures under large shear deformation causing their volume expansion (thus transformation to low-density phases) with reduced ideal shear strengths below that of diamond. At high pressure, however, transformations to low-density phases are suppressed and the structural changes are redirected toward high-density phases that possess ideal shear strengths that are higher than that of diamond in its weakest shear direction. Since all the proposed compressed graphite phases have the same building blocks ($5+7$ or $4+8$ membered rings) similar to those in W-, M-, and Z-carbon, the same trends and conclusions are expected to hold for all these carbon allotropes.

In recent years, several empirical formulas have been proposed and widely used to estimate material hardness.[27–30] They use material parameters at equilibrium under ambient conditions as input and extrapolate to large-strain states via empirical parametrization to estimate hardness. While such formulas offer a convenient approach with reasonable

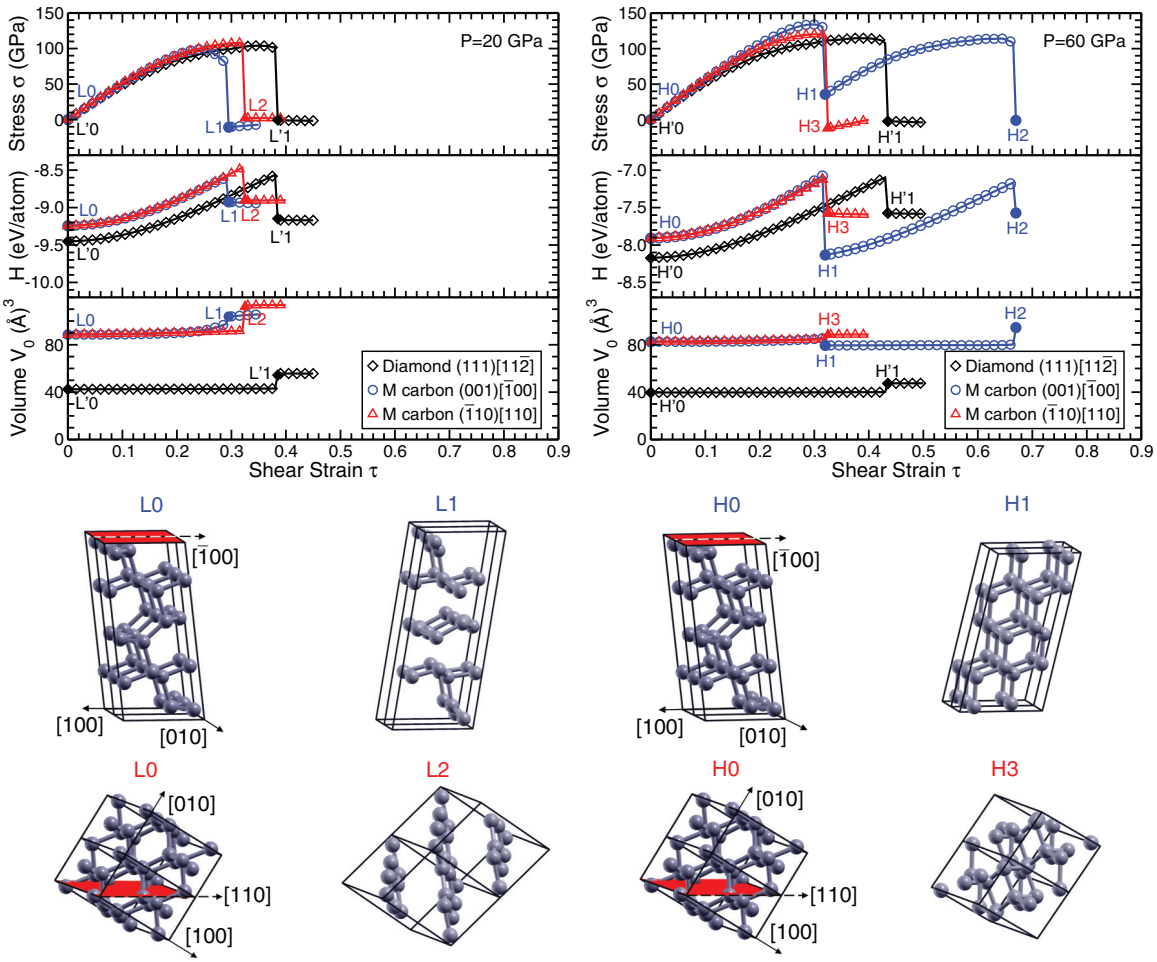

FIG. 3. (Color online) Calculated stress (upper panel), enthalpy (middle panel), and unit cell volume (lower panel) of M-carbon versus strain in the (001)[$\bar{1}$00] and ($\bar{1}$10)[110] shear directions (shear sliding planes are shaded) at 20 and 60 GPa compared to those of diamond in the (111)[11$\bar{2}$] shear direction. Also given are selected structural snapshots of M-carbon during shear deformation. The unit cell of M-carbon contains 16 carbon atoms.

accuracy when applied to known material structures after initial calibration, they suffer catastrophic failures when key material aspects, such as strong structural anisotropy, are not considered[30] or subtle charge-state changes render the

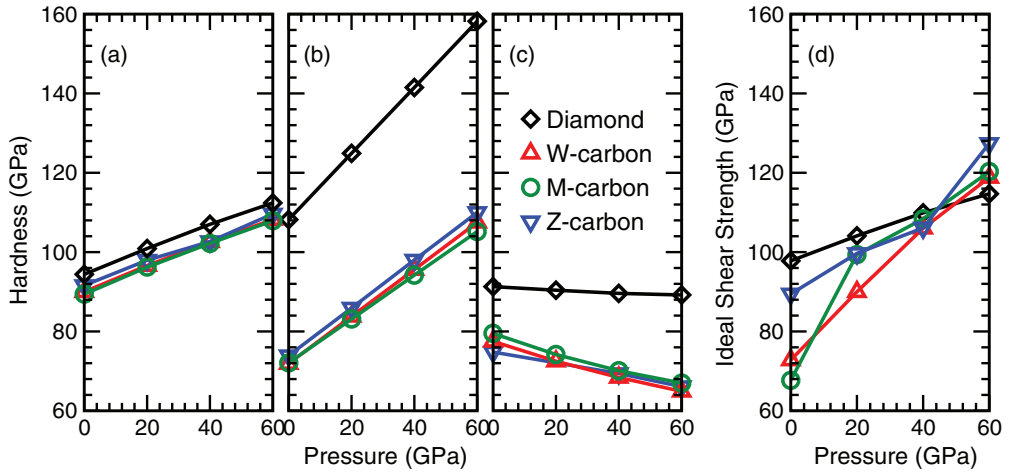

FIG. 4. (Color online) Hardness of diamond, W-carbon, M-carbon, and Z-carbon as functions of pressure estimated using the empirical formula proposed by (a) Simunek (Ref. 28), (b) Mukhanov (Ref. 29), and (c) Chen (Ref. 30), in comparison with (d) the calculated ideal shear strength.

parametrization unreliable.[38] The behavior of compressed graphite offers an exemplary case study. We show in Fig. 4 the hardness of W-, M-, and Z-carbon and diamond versus pressure calculated using three different types of empirical formulas[28–30] compared to our first-principles ideal shear strength, which is known to correlate well with measured hardness[3,4] and set a fundamental trend for the strength-pressure relation. The results show that all three empirical formulas give incorrect trends: one formula[30] shows a qualitatively incorrect (negative) pressure dependence, while the other two[28,29] fail to predict the faster increase of hardness over that of diamond at high pressure. None of them predict that compressed graphite becomes harder than diamond at high pressure as observed in experiment.[12] First-principles stress-strain calculations are required to capture qualitatively different high pressure structural deformation modes and their effect on strength and hardness.

In summary, we show by first-principles calculations that high-pressure constraint suppresses the usual ambient or low-pressure shear deformation modes and promotes new mechanisms that lead to unexpectedly large strength enhancement of compressed graphite, making it stronger than diamond. This finding explains the puzzling experimental observation of compressed graphite cracking diamond anvil. These results suggest different principles for understanding constrained structural evolution at high pressure; they also highlight the limitation of widely used empirical hardness formulas and underscore the need for a more sophisticated and reliable first-principles approach in exploring new materials, especially under extreme conditions such as high pressure, when unexpected structural changes are likely to occur.

This work was supported by DOE Grant No. DE-FC52-06NA26274 at UNLV and NNSF of China Grant No. 11174200 at SJTU. H.S. also appreciates the support of the Science and Engineering Interdisciplinary Research Foundation of SJTU.

*Corresponding author: hsun@sjtu.edu.cn
†Corresponding author: chen@physics.unlv.edu

[1] S. Ogata, J. Li, and S. Yip, Science **298**, 807 (2002).
[2] X. Blase, P. Gillet, A. San Miguel, and P. Mélinon, Phys. Rev. Lett. **92**, 215505 (2004).
[3] Y. Zhang, H. Sun, and C. F. Chen, Phys. Rev. Lett. **93**, 195504 (2004).
[4] Y. Zhang, H. Sun, and C. F. Chen, Phys. Rev. Lett. **94**, 145505 (2005).
[5] M. G. Fyta, I. N. Remediakis, P. C. Kelires, and D. A. Papaconstantopoulos, Phys. Rev. Lett. **96**, 185503 (2006).
[6] Z. C. Pan, H. Sun, and C. F. Chen, Phys. Rev. Lett. **98**, 135505 (2007).
[7] Z. C. Pan, H. Sun, Y. Zhang, and C. F. Chen, Phys. Rev. Lett. **102**, 055503 (2009).
[8] W. Zhou, H. Sun, and C. F. Chen, Phys. Rev. Lett. **105**, 215503 (2010).
[9] J. Li, K. J. Van Vliet, T. Zhu, S. Yip, and S. Suresh, Nature (London) **418**, 307 (2002).
[10] W. Utsumi and T. Yagi, Science **252**, 1542 (1991).
[11] E. D. Miller, D. C. Nesting, and J. V. Badding, Chem. Mater. **9**, 18 (1997).
[12] W. L. Mao, H. Mao, P. J. Eng, T. P. Trainor, M. Newville, C. Kao, D. L. Heinz, J. Shu, Y. Meng, and R. J. Hemley, Science **302**, 425 (2003).
[13] Q. Li, Y. Ma, A. R. Oganov, H. Wang, H. Wang, Y. Xu, T. Cui, H.-K. Mao, and G. Zou, Phys. Rev. Lett. **102**, 175506 (2009).
[14] K. Umemoto, R. M. Wentzcovitch, S. Saito, and T. Miyake, Phys. Rev. Lett. **104**, 125504 (2010).
[15] J.-T. Wang, C. Chen, and Y. Kawazoe, Phys. Rev. Lett. **106**, 075501 (2011); Phys. Rev. B **84**, 012102 (2011).
[16] X. L. Sheng, Q. B. Yan, F. Ye, Q. R. Zheng, and G. Su, Phys. Rev. Lett. **106**, 155703 (2011).
[17] Z. Zhao, B. Xu, X.-F. Zhou, L.-M. Wang, B. Wen, J. He, Z. Liu, H.-T. Wang, and Y. Tian, Phys. Rev. Lett. **107**, 215502 (2011).
[18] M. Amsler, J. A. Flores-Livas, L. Lehtovaara, F. Balima, S. A. Ghasemi, D. Machon, S. Pailhès, A. Willand, D. Caliste, S. Botti, A. San Miguel, S. Goedecker, and M. A. L. Marques, Phys. Rev. Lett. **108**, 065501 (2012).
[19] H. Niu, X.-Q. Chen, S. Wang, D. Li, W. L. Mao, and Y. Li, Phys. Rev. Lett. **108**, 135501 (2012).
[20] R. Zhou and X. C. Zeng, J. Am. Chem. Soc. **134**, 7530 (2012).
[21] Q. Zhu, Q. Zeng, and A. R. Oganov, Phys. Rev. B **85**, 201407 (2012).
[22] Q. Zhu, A. R. Oganov, M. A. Salvado, P. Pertierra, and A. O. Lyakhov, Phys. Rev. B **83**, 193410 (2011).
[23] S. E. Boulfelfel, A. R. Oganov, and S. Leoni, Sci. Rep. **2**, 471 (2012).
[24] Y. J. Wang, J. E. Panzik, B. Kiefer, and K. K. M. Lee, Sci. Rep. **2**, 520 (2012).
[25] R. F. Zhang, Z. J. Lin, and S. Veprek, Phys. Rev. B **83**, 155452 (2011).
[26] Z. Li, F. Gao, and Z. Xu, Phys. Rev. B **85**, 144115 (2012).
[27] F. Gao, J. He, E. Wu, S. Liu, D. Yu, D. Li, S. Zhang, and Y. Tian, Phys. Rev. Lett. **91**, 015502 (2003).
[28] A. Šimůnek and J. Vackář, Phys. Rev. Lett. **96**, 085501 (2006).
[29] V. A. Mukhanova, O. O. Kurakevycha, and V. L. Solozhenko, Philos. Mag. **89**, 2117 (2009).
[30] X. Q. Chen, H. Niu, C. Franchini, D. Li, and Y. Li, Phys. Rev. B **84**, 121405 (2011).
[31] See the website http://www.vasp.at/.
[32] P. E. Blöchl, Phys. Rev. B **50**, 17953 (1994); G. Kresse and D. Joubert, *ibid*. **59**, 1758 (1999).
[33] D. M. Ceperley and B. J. Alder, Phys. Rev. Lett. **45**, 566 (1980).
[34] J. P. Perdew and Y. Wang, Phys. Rev. B **45**, 13244 (1992).
[35] M. P. Teter, M. C. Payne, and D. C. Allan, Phys. Rev. B **40**, 12255 (1989); D. M. Bylander, L. Kleinman, and S. Lee, Phys Rev. B **42**, 1394 (1990).
[36] H. J. Monkhorst and J. D. Pack, Phys. Rev. B **13**, 5188 (1976).
[37] B. Zhang and W. Guo, Appl. Phys. Lett. **87**, 051907 (2005).
[38] R. F. Zhang, D. Legut, Z. J. Lin, Y. S. Zhao, H. K. Mao, and S. Veprek, Phys. Rev. Lett. **108**, 255502 (2012).